mathematics

MDPI

Article

Event-Triggered Impulsive Control for Switched Systems Under Aperiodic Denial-of-Service Attacks

Ting Zhuang, Shuo Yin, Xiaoyu Zhang * and Jilu Wang

School of Information Science and Technology, Beijing Foreign Studies University, Beijing 100089, China; 202320119011@bfsu.edu.cn (T.Z.); 202520229005@bfsu.edu.cn (S.Y.); jiluwang@bfsu.edu.cn (J.W.)
* Correspondence: zxymath@bfsu.edu.cn

Abstract

Ensuring input-to-state stability (ISS) of networked control systems under simultaneous mode switching and cyber attacks is a challenging open problem, since the asynchronous interplay among continuous dynamics, event-triggered impulses, and aperiodic denial-of-service (DoS) blockages has not been addressed in a unified nonlinear framework. This paper establishes such a framework by integrating a mode-dependent event-triggered mechanism (MDETM) with the admissible edge-dependent average dwell time (AED-ADT) approach for continuous-time nonlinear impulsive switched systems. Under mild Lyapunov-based conditions, rigorous sufficient conditions are derived that (i) guarantee a strictly positive uniform inter-event lower bound $\underline{\Delta} > 0$, and (ii) establish global ISS with an explicit exponential decay rate $\eta > 0$ that quantifies the trade-offs among the AED-ADT limit, the DoS frequency/duration parameters (τ_D, τ_d), and the triggering coefficients (a_k, d_k). The nonlinear framework is further specialized to linear systems, yielding tractable Linear Matrix Inequality (LMI) criteria. Numerical validation on a two-subsystem linear impulsive switched system confirms the theoretical predictions: the LMI solver returns $\eta = 0.451$, a Zeno-free lower bound $\Delta_1 = 0.0103\,\mathrm{s}$, and the state converges from $x(t_0) = [100, -100]^\top$ to $\|x(10)\| = 0.0011$ under an average DoS duty cycle of approximately 15%.

Keywords: switched systems; event-triggered impulsive control; DoS; AED-ADT; ISS

MSC: 39D05

1. Introduction

In many practical scenarios, it is essential to consider the behavior of networked control systems (NCSs) operating under malicious cyber threats over a finite period. For instance, in complex industrial automation or chemical processes, maintaining system states within prescribed safe bounds is critical despite unpredictable network interruptions. To address such challenges, De Persis and Tesi [1] introduced the foundational concept of ISS control under DoS attacks. Dolk et al. [2] further emphasized that DoS attacks pose a significantly more severe challenge to closed-loop stability compared to traditional time-triggered control, primarily because they interrupt system operations aperiodically. Recently, the concept of DoS resilience—defined as the capability to preserve ISS despite prolonged communication blockages—has been extensively explored in literature such as [3,4]. A great variety of research has been devoted to this field due to its wide range of practical applications, where resilient event-triggered schemes and switching signal reconstruction are utilized to mitigate attack-induced instability.

Check for updates

Academic Editor: Pierpaolo Soravia

Received: 11 May 2026
Revised: 20 June 2026
Accepted: 23 June 2026
Published: 3 July 2026

Copyright: © 2026 by the authors. Licensee MDPI, Basel, Switzerland. This article is an open access article distributed under the terms and conditions of the Creative Commons Attribution (CC BY) license.

Event-triggered control (ETC) has emerged as an indispensable methodology for investigating NCSs with limited communication bandwidth, such as satellite orbit transitions and secure communication systems [5,6]. By updating control inputs only when specific state-dependent conditions are violated, the event-triggered mechanism (ETM) provides a natural framework for managing systems with discontinuous control updates. Since the foundational results presented by Tabuada [5], the domain of ETC has been a focal point of research for decades, particularly regarding the stability and resource efficiency of networked dynamics. Current research generally branches into two categories: approaches utilizing fixed-threshold impulses [7] and those focusing on mode-dependent or dynamic event-triggered mechanisms [8]. The integration of ETC with impulsive control has yielded significant breakthroughs, such as the Lyapunov stability analysis for impulsive systems via ETC and the investigation of nonlinear delay systems using comparison principles [7]. In the context of ETC, various fundamental methodologies have been proposed, including event-separation properties [9] and co-design perspectives for efficient communication [10]. Multiagent consensus via ETC has also drawn significant attention [11–13]. Furthermore, Zeno-free dynamic surface control and impulsive mechanisms have been tailored to address continuous-time nonlinear networks [14,15].

Robust control approaches for perturbed nonlinear systems—including sliding-mode extremum seeking with barrier functions [16] and observer-based designs for electric-vehicle drives under unmatched load disturbances [17]—further motivate the need for systematic NCS frameworks that simultaneously handle cyber threats and unmatched disturbances.

Asynchronous behavior is a critical concept used to depict the scenario where system mode switching and impulsive updates are mutually independent and generally do not coincide. Switched systems, as a vital class of hybrid systems, exhibit intermittent state jumps during their continuous evolution [18]. To systematically handle the resulting asynchrony, the average dwell time (ADT) approach [19] and its generalization, the AED-ADT [20], have become indispensable analytical tools. Since the initial inception of the ADT framework [21], it has been vastly adapted for hybrid systems experiencing cyber-attacks [22]. Exploring the resilience of NCSs, extensive literature now focuses on H_∞ synchronization [23], resilient mechanisms under periodic blockages [24], quantized tracking [25], and comprehensive security control surveys [26] under DoS attacks. In complex real-world environments, systems frequently endure multimodal switching and malicious attacks simultaneously. Under DoS attacks, the blocked impulses force the system state to depend heavily on the historical trajectory during the attack's active period [27]. While early literature modeled impulsive delays as fixed or integral-based, recent studies recognize that attack-induced blockages vary dynamically across different triggering instants [27,28]. This operational need led to the development of the MDETM [29], where triggering thresholds adapt based on the active system mode and attack status. Related work. Several closely related lines of research deserve detailed discussion. Regarding ISS under DoS attacks, De Persis and Tesi [1] laid the foundations for stabilizing control under denial-of-service, while Dolk et al. [2] extended this to event-triggered control systems. More recent contributions [3,4] address resilient event-triggered schemes for switched systems under DoS blockages, yet both assume synchronous triggering mechanisms without mode-dependent threshold adaptation. On the impulsive control side, existing studies [7,8] provide Lyapunov stability criteria for event-triggered impulsive systems, but do not consider network attacks. The hybrid schemes in [27,28] handle DoS attacks with impulsive components, yet are restricted to multi-agent consensus topologies and do not cover the ISS of general single switched systems. The MDETM was introduced in [29] for mode-dependent dynamic event-triggered impulsive control, but that work operates

under classical average dwell-time assumptions with synchronous switching-impulse interactions. In the broader security control literature, comprehensive surveys [26] identify fully asynchronous nonlinear impulsive switched systems as an open class that current frameworks do not subsume. The present paper fills this gap, as detailed below.

However, existing works such as [3,4] primarily address ISS under DoS attacks for systems without mode-dependent triggering mechanisms. Although refs. [27,28] investigate hybrid event-triggered and impulsive control under cyber-attacks, their cluster of results is restricted to multi-agent consensus topologies rather than the explicit ISS analysis of general single switched systems. Furthermore, ref. [29] introduces the MDETM yet operates under the assumption of synchronous switching-impulse interactions or classical dwell-time frameworks, failing to capture the fully asynchronous decoupling between mode-switching and impulse updates characterized by the AED-ADT framework. To the best of the authors' knowledge, a comprehensive theoretical framework simultaneously integrating MDETM, asynchronous switching via AED-ADT, and DoS resilience for continuous-time nonlinear impulsive switched systems remains largely unexplored.

Hinted by the above discussion, we investigate the problem of event-triggered impulsive control for continuous-time nonlinear impulsive switched systems subject to aperiodic DoS attacks. The main contributions of this paper are explicitly summarized as follows:

- Unified nonlinear framework: This paper is the first to simultaneously integrate MDETM, asynchronous mode switching via AED-ADT and aperiodic DoS resilience for continuous-time nonlinear impulsive switched systems. Specifically, [3,4] achieve ISS under DoS without mode-dependent triggering; [27,28] combine event-triggered impulses with DoS but are confined to cooperative multi-agent networks; and [29] introduces MDETM yet restricts it to synchronous switching or classical ADT. The proposed framework simultaneously handles all three challenges in a single general nonlinear continuous-time setting.
- Zeno-free MDETM with explicit lower bound: Under the adopted MDETM (2)–(3), the triggering threshold adapts to both the active Lyapunov function and a class-$\mathcal{K}_\infty$ upper bound on disturbances. A positive uniform inter-event lower bound $\underline{\Delta} > 0$ is derived analytically (Theorem 1), confirming Zeno-free operation without requiring smoothness assumptions on inter-event intervals.
- Explicit ISS decay-rate formula: Through impulsive differential equations [30] and the AED-ADT approach, the Lyapunov function is estimated under the simultaneous influence of asynchronous switching and aperiodic DoS blockages. Condition (VI) yields a closed-form exponential decay rate (see Theorem 2) that makes the trade-offs among the AED-ADT limit, the DoS frequency/duration parameters, and the triggering coefficients fully transparent.
- Tractable LMI criteria for linear systems: The nonlinear framework is specialized to linear impulsive switched systems (Theorem 3), yielding LMI conditions amenable to standard solvers (e.g., YALMIP/MOSEK) and facilitating direct controller design.

The rest of this article is structured as follows. Section 2 formulates the problem and introduces essential definitions regarding the DoS model and AED-ADT; Section 3 details the rigorous analysis of Zeno behavior exclusion and establishes the ISS criteria for both nonlinear and linear cases; Section 4 provides a comprehensive numerical example to validate the theoretical findings; and Section 5 concludes the paper together with future work.

2. Problem Formulation and Preliminaries

Consider the following continuous-time nonlinear impulsive switched system:

$$\begin{cases} \dot{x}(t) = f_{\sigma(t)}(x(t), \omega(t)), & t \geq t_0, \quad t \notin \{t_k \mid k \in \mathbb{Z}_+\}, \\ x(t_k) = h_k(x(t_k^-)), & k \in \mathbb{Z}_+, \end{cases} \tag{1}$$

where $x(t) \in \mathbb{R}^n$ is the system state with the initial value $x(t_0) = x_0$; $\omega(t) \in \mathbb{R}^m$ is the bounded external continuous disturbance input; $\sigma(t) \in \Omega$ is a right-continuous, piecewise constant switching signal, where Ω is a finite index set. The switching time sequence is denoted as $\mathcal{S} = \{t_s^k \mid s, k \in \mathbb{Z}_+\}$, satisfying $t_{k-1} < t_1^k < t_2^k < \cdots < t_m^k < t_k$. The switching instants $\{t_s^k\}$ and the triggering impulsive instants $\{t_k\}$ are independent of each other and generally do not coincide. The continuous dynamics $f_i : \mathbb{R}^n \times \mathbb{R}^m \to \mathbb{R}^n$ and state jumps $h_k : \mathbb{R}^n \to \mathbb{R}^n$ satisfy the local Lipschitz condition, with $f_i(0, 0) = 0$ and $h_k(0) = 0$.

For system (1), the following MDETM is adopted:

$$t_k = \inf\{t > t_{k-1} \mid \phi_{k-1}(t) \geq 0\}, \tag{2}$$

The overall structure of the proposed control system is illustrated in Figure 1, where the triggering function is defined as

$$\phi_{k-1}(t) = V_{\sigma(t)}(t, x(t)) - e^{a_k} V_{\sigma(t_{k-1})}(t_{k-1}, x(t_{k-1})) - e^{b_k} \chi(\|\omega\|_{[t_{k-1}, t]}), \tag{3}$$

with $a_k, b_k \in \mathbb{R}_+$ as triggering parameters, $V_i(t, x)$ the Lyapunov function of the i-th subsystem, and χ a class-$\mathcal{K}_\infty$ function. The interval t_{k-1} is the last successful triggering instant, initially $t_{-1} = t_0$.

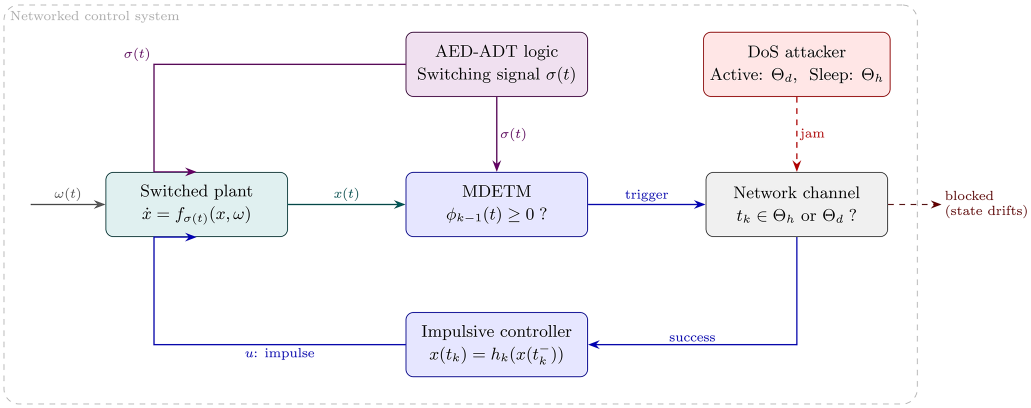


Figure 1. Block diagram of the proposed MDETM-based event-triggered impulsive control system under aperiodic DoS attacks. The MDETM monitors state $x(t)$ and switching signal $\sigma(t)$ to generate trigger attempts, which are transmitted through the network channel. During DoS sleeping intervals Θ_h, impulses are successfully applied as $x(t_k) = h_k(x(t_k^-))$; during active intervals Θ_d, transmissions are blocked and the state evolves freely.

Remark 1. *The switching signal $\sigma(t)$ is generated by an external scheduler and evolves independently of the MDETM. Specifically, the triggering mechanism in (2) uses $\sigma(t)$ to select the active Lyapunov function $V_{\sigma(t)}$ but does not influence the switching sequence $\{t_s^k\}$. This one-way dependence ensures that the asynchronous interaction between mode switches and impulsive events is well-posed: at any switching instant t_s^k, the state is continuous, no jump occurs due to the switch alone, while the MDETM clock t_{k-1} continues from the last successful impulse instant.*

Definition 1. *System (1) is ISS if there exist $\beta \in \mathcal{KL}$ and $\gamma \in \mathcal{K}$ such that for any bounded disturbance $\omega(t)$ and $x(t_0) = x_0$:*

$$|x(t)| \leq \beta(|x_0|, t - t_0) + \gamma(\|\omega\|_{[t_0,t]}), \quad \forall t \geq t_0.$$

Definition 2. *An aperiodic DoS attack is characterized by active intervals $D_n = [h_n, h_n + d_n)$ and sleeping intervals $H_n = [h_n + d_n, h_{n+1})$. The total active and sleeping subsets over $[t_0, t)$ are:*

$$\Theta_d(t_0, t) = \bigcup_{n\in\mathbb{N}} D_n \cap [t_0, t), \quad \Theta_h(t_0, t) = [t_0, t) \setminus \Theta_d(t_0, t).$$

During $\Theta_d(t_0, t)$, event-triggered impulses are invalidated. The continuous dynamics remain subject to $\omega(t)$, and $\sigma(t)$ evolves independently.

Definition 3. *The number of DoS attacks $N_d(t_0, t)$ within $[t_0, t)$ satisfies:*

$$N_d(t_0, t) \leq N_0 + \frac{t - t_0}{\tau_D}, \quad N_0 > 0, \tau_D > 0. \tag{4}$$

Definition 4. *The total duration of active periods $|\Theta_d(t_0, t)|$ satisfies:*

$$|\Theta_d(t_0, t)| \leq \theta_0 + \frac{t - t_0}{\tau_d}, \quad \theta_0 > 0, \tau_d > 1. \tag{5}$$

Definition 5. *Let $N^{\sigma}_{j,i}(t, t_0)$ denote the switches from subsystem j to i over $[t_0, t)$, and $T_{j,i}(t, t_0)$ the running time of i after switching from j. If there exist $N^{\sigma,0}_{j,i} > 0$ and $\tau^{\sigma}_{j,i} > 0$ such that*

$$N^{\sigma}_{j,i}(t, t_0) \leq N^{\sigma,0}_{j,i} + \frac{T_{j,i}(t, t_0)}{\tau^{\sigma}_{j,i}}, \quad \forall t \geq t_0 \geq 0, \tag{6}$$

then $\tau^{\sigma}_{j,i}$ is the AED-ADT with chatter bound $N^{\sigma,0}_{j,i}$.

Definition 6. *Let M be the total triggers over $[t_0, t)$, and N the failed triggers due to DoS. The successful impulse ratio $\rho \in (0, 1]$ is:*

$$\rho = \frac{M - N}{M}. \tag{7}$$

Remark 2. *The proposed framework handles both matched and unmatched external disturbances. In the nonlinear setting (1), the disturbance input $\omega(t)$ enters through $f_i(x, \omega)$. In the linear setting (17), the input matrix B_i is not required to equal the control input matrix; it can represent an unmatched disturbance channel. The LMI condition (VII) absorbs B_i directly via the Schur complement, so no structural assumption on the disturbance channel is needed.*

Notation. Throughout this paper, we adopt the following conventions. $\mathbb{R}^n$ denotes the n-dimensional Euclidean space; $|\cdot|$ denotes the Euclidean norm of a vector. For a measurable signal $v : [a, b] \to \mathbb{R}^m$, we write $\|v\|_{[a,b]} := \operatorname{ess\,sup}_{t\in[a,b]} |v(t)|$ for its L^∞-norm on the interval $[a, b]$. For two real numbers p, q, we write $p \wedge q := \min\{p, q\}$. The triggering parameter $a_k \in \mathbb{R}_+$ controls the decay threshold: it scales the Lyapunov value at the previous trigger instant, determining how much the Lyapunov function may grow before a new trigger is required. The triggering parameter $b_k \in \mathbb{R}_+$ controls the disturbance tolerance: it scales the disturbance upper bound in the triggering condition. The impulse decay parameter $d_k \in \mathbb{R}_+$ (distinct from a_k) characterizes the stabilizing effect of each impulse via condition condition (V).

The switching time sequence $\mathcal{S} = \{t_s^k \mid s, k \in \mathbb{Z}_+\}$ uses the superscript k to index the triggering interval and the subscript s to index the switching instant within that interval; t_k with no superscript denotes the k-th successful impulsive triggering instant. Constants $\tilde{K}_1$ (no-DoS case) and $\tilde{K}$ (with-DoS case) in the ISS proof are distinct composite bounds defined in Cases 1 and 2 of the Theorem 2 proof, respectively; $\tilde{K}_1$ is a special case of $\tilde{K}$ when $\ell_k^d = 0$. The overall implementation procedure of the proposed MDETM-based impulsive control under aperiodic DoS attacks is summarized in Algorithm 1.

Algorithm 1 MDETM-based Event-Triggered Impulsive Control under Aperiodic DoS Attacks

Require: System matrices, Lyapunov matrices $\{P_i\}$, parameters $a_k, b_k, d_k, \Delta_{\max}$, DoS model parameters τ_D, τ_d
Ensure: State trajectory $x(t)$ satisfying ISS
Initialize: $t_{-1} \leftarrow t_0, k \leftarrow 0$
while $t < T$ **do**
  Observe current state $x(t)$ and active mode $\sigma(t)$
  Evaluate: $\phi_{k-1}(t) = V_{\sigma(t)}(t, x(t)) - e^{a_k} V_{\sigma(t_{k-1})}(t_{k-1}, x(t_{k-1})) - e^{b_k}\chi(\|\omega\|_{[t_{k-1},t]})$
  if $\phi_{k-1}(t) \geq 0$ **or** $t - t_{k-1} \geq \Delta_{\max}$ **then**
    Trigger attempt at $t_k \leftarrow t$
    if $t_k \in \Theta_h(t_0, t)$ **then** ▷ DoS sleeping: channel available
      Apply impulse: $x(t_k) \leftarrow h_k(x(t_k^-))$
      Update: $t_{k-1} \leftarrow t_k; k \leftarrow k+1$
    else ▷ DoS active: channel blocked
      Discard impulse; state evolves under $\dot{x} = f_{\sigma(t)}(x, \omega)$
    end if
  end if
  Integrate $\dot{x} = f_{\sigma(t)}(x(t), \omega(t))$ to next event or $t + \Delta t$
end while

3. Main Results

3.1. Exclusion of Zeno Behavior

Theorem 1. *Consider system* (1). *Suppose there exist a function* $V : \mathbb{R}^n \times \mathbb{R}^n \to \mathbb{R}_+$, *class-*$\mathcal{K}_\infty$ *functions* α_1, α_2, χ, *and constants* $\lambda_i \in \mathbb{R}_+$, $\mu_{j,i} \geq 1$, $a_k, b_k \in \mathbb{R}_+$, *such that for all* $i, j \in \Omega$:

(I) $D^+V_i(t, x(t)) \leq \lambda_i V_i(t, x(t)) + \chi(|\omega(t)|), \quad t \in [t_{k-1}, t_k)$;
(II) $V_i(t, x(t)) \leq \mu_{j,i} V_j(t, x(t^-)) + \chi(|\omega(t)|), \quad t \in \mathcal{S}$;
(III) $\inf_{k \in \mathbb{Z}_+} \{\ln(e^{a_k} \wedge e^{b_k})\} > \bar{\gamma} + \sum_{j,i} N_{j,i}^{\sigma,0} \ln \mu_{j,i}$,

where $\bar{\gamma} = \ln 3 \cdot \sum_{j,i} N_{j,i}^{\sigma,0}$. *Then, under MDETM* (2), *the system exhibits no Zeno behavior.*

Proof. For any adjacent triggering interval $[t_{k-1}, t_k)$, the condition $\phi_{k-1}(t) < 0$ implies:

$$V_{\sigma(t_k^-)}(t_k^-, x(t_k^-)) = e^{a_k} V_{\sigma(t_{k-1})}(t_{k-1}, x(t_{k-1})) + e^{b_k}\chi(\|\omega\|_{[t_{k-1},t_k]}). \tag{8}$$

Case 1: No switching instants t_s^k occur within $[t_{k-1}, t_k)$. By condition (I) and Gronwall's inequality [31], taking $t \to t_k^-$, we have:

$$\begin{aligned} V_i(t, x(t)) &\leq e^{\lambda_i(t-t_{k-1})} V_i(t_{k-1}, x(t_{k-1})) + \int_{t_{k-1}}^{t} e^{\lambda_i(t-s)}\chi(|\omega(s)|)ds \\ &\leq e^{\lambda_i(t-t_{k-1})} V_i(t_{k-1}, x(t_{k-1})) + \frac{e^{\lambda_i(t-t_{k-1})} - 1}{\lambda_i}\chi(\|\omega\|_{[t_{k-1},t_k]}). \end{aligned} \tag{9}$$

Combining (8) and (9), and utilizing $e^{a_k} \wedge e^{b_k} \leq \min(e^{a_k}, e^{b_k})$, we obtain:

$$t_k - t_{k-1} \geq \frac{1}{\lambda_i} \ln \frac{(e^{a_k} \wedge e^{b_k})\lambda_i + 1}{\lambda_i + 1} =: \Delta_1 > 0.$$

Case 2: Switching instants $t_{k-1} < t_1^k < \cdots < t_m^k < t_k$ exist. Let $t_0^k = t_{k-1}$ and denote the Gronwall coefficient for each sub-interval $s \in \{1, \ldots, m+1\}$ as:

$$G^{(s)} := \frac{(\lambda_{\sigma(t_{s-1}^k)} + 1)e^{\lambda_{\sigma(t_{s-1}^k)}(t_s^k - t_{s-1}^k)} - 1}{\lambda_{\sigma(t_{s-1}^k)}}.$$

Define $W_k := \chi(\|\omega\|_{[t_{k-1}, t_k]})$ and $A_s := V_{\sigma(t_s^k)}(t_s^k, x(t_s^k)) + W_k$. Applying conditions (I) and (II) iteratively across switches yields:

$$A_s \leq \left(\mu_{\sigma(t_{s-1}^k),\sigma(t_s^k)} G^{(s)} + 2\right) A_{s-1} =: Q_s A_{s-1}, \quad s = 1, \ldots, m.$$

Consequently, $A_m \leq \prod_{s=1}^m Q_s A_0$. For the final interval $[t_m^k, t_k)$:

$$V_{\sigma(t_k^-)}(t_k^-, x(t_k^-)) \leq G^{(m+1)} \prod_{s=1}^m Q_s A_0. \tag{10}$$

Substituting A_0 into (8) provides $V_{\sigma(t_k^-)}(t_k^-, x(t_k^-)) \geq (e^{a_k} \wedge e^{b_k}) A_0$. Combining this with (10) gives:

$$e^{a_k} \wedge e^{b_k} \leq G^{(m+1)} \prod_{s=1}^m \left(\mu_{\sigma(t_{s-1}^k),\sigma(t_s^k)} G^{(s)} + 2\right) =: R(\{\Delta_s\}). \tag{11}$$

We now prove Case 2 rigorously via a contradiction argument. Each Gronwall coefficient $G^{(s)}$ depends continuously on the sub-interval length $\Delta_s^k := t_s^k - t_{s-1}^k$ and satisfies $G^{(s)}\big|_{\Delta_s^k = 0} = 1$; in particular, $G^{(s)} \geq 1$ is strictly increasing in Δ_s^k. Hence, there exists a continuous function $g : \mathbb{R}_+ \to \mathbb{R}_+$ with $g(0) = 0$ such that $G^{(s)} \leq 1 + g(\Delta_k)$ for all s, where $\Delta_k := t_k - t_{k-1}$. By AED-ADT (6), when $\Delta_k \to 0^+$ the switch count satisfies $m \leq \bar{M} := \sum_{j,i} N_{j,i}^{\sigma,0}$ for all sufficiently small Δ_k.

Suppose for contradiction that $\Delta_k \to 0^+$ along some subsequence. Since the product $R(\{\Delta_s\}) = G^{(m+1)} \prod_{s=1}^m Q_s$ is a finite product of continuous functions with $m \leq \bar{M}$ uniformly bounded, continuity gives

$$R(\{\Delta_s\}) \xrightarrow{\Delta_k \to 0^+} L := \prod_{s=1}^{\bar{M}} (\mu_{\sigma(t_{s-1}^k),\sigma(t_s^k)} + 2),$$

Taking logarithms and using $\ln(\mu + 2) \leq \ln 3 + \ln \mu$ for $\mu \geq 1$:

$$\ln L \leq \ln 3 \sum_{j,i} N_{j,i}^{\sigma,0} + \sum_{j,i} N_{j,i}^{\sigma,0} \ln \mu_{j,i} = \bar{\gamma} + \sum_{j,i} N_{j,i}^{\sigma,0} \ln \mu_{j,i},$$

By condition (III), $\inf_k (e^{a_k} \wedge e^{b_k}) \geq L + \varepsilon$ for some $\varepsilon > 0$. By continuity of R, there exists $\delta > 0$ such that $R < L + \varepsilon$ whenever $\Delta_k < \delta$. Then, (11) gives $L + \varepsilon \leq e^{a_k} \wedge e^{b_k} \leq R < L + \varepsilon$, a contradiction. Therefore, $t_k - t_{k-1} \geq \Delta_2 := \delta > 0$.

Let $\underline{\Delta} = \min\{\Delta_1, \Delta_2\} > 0$, confirming the exclusion of Zeno behavior.

Since $\underline{\Delta} = \min\{\Delta_1, \Delta_2\} > 0$ is a *uniform* lower bound on all inter-event intervals $t_k - t_{k-1}$, there can be no accumulation point of the sequence $\{t_k\}$ in finite time. Therefore, Zeno behavior—defined as infinitely many triggering events in a finite interval—is rigorously excluded. □

3.2. ISS of Nonlinear Systems Under DoS Attacks

Theorem 2. *Based on conditions (I)–(III) of Theorem 1 and assuming the existence of $\underline{\Delta}$, consider the nonlinear impulsive switched system (1). Suppose there exist a function $V : \mathbb{R}^n \times \mathbb{R}^n \to \mathbb{R}_+$, class-$\mathcal{K}_\infty$ functions α_1, α_2, χ, and a positive constant Δ_{max}, such that for $\forall k \in \mathbb{Z}_+$, the adjacent successful*

triggering instants generated by the MDETM (2) satisfy: $t_k - t_{k-1} \leq \Delta_{max}$, $\sup_{k\in\mathbb{Z}_+} a_k \leq \bar{a} < +\infty$, $\sup_{k\in\mathbb{Z}_+} b_k \leq \bar{b} < +\infty$. *Also assume there exist constants* $d_k > 0$, $\lambda_i \in \mathbb{R}_+$, *and* $\mu_{j,i} \geq 1$, *such that for all* $i, j \in \Omega$, *the following conditions hold:*

(IV) $\alpha_1(|x|) \leq V_i(t,x) \leq \alpha_2(|x|)$;

(V) $V_{\sigma(t_k)}(t_k, x(t_k)) \leq e^{-d_k} \cdot V_{\sigma(t_k^-)}(t_k^-, x(t_k^-))$;

(VI) $$\frac{d_{\min}}{\Delta_{max}}\left(1 - \frac{1}{\tau_d}\right) - \frac{d_{\min}}{\tau_D} - \frac{\bar{a}}{\underline{\Delta}} - \frac{\bar{\lambda}}{\tau_d} > 0,$$

where $\bar{\lambda} = \max_{i\in\Omega} \lambda_i$, $d_{\min} = \inf_k\{d_k\} > 0$. *Then, under the MDETM (2)–(3), system (1) is ISS.*

Proof. Let $\ell_k^d := |\Theta_d(t_0, t_k) \cap [t_{k-1}, t_k]| \geq 0$ be the total DoS active duration within interval $[t_{k-1}, t_k]$, and $\chi_k := \chi(\|\omega\|_{[t_{k-1},t_k]})$.

We decompose each successful triggering interval $[t_{k-1}, t_k]$ into three sub-arcs:

- Sleeping sub-arcs $[t_{k-1}, t_k] \cap \Theta_h$ (total length $\ell_k^h = \Delta_k - \ell_k^d$): the MDETM condition $\phi_{k-1}(t) < 0$ holds and no impulse fires, so the state evolves under $f_{\sigma(t)}$ with the triggering bound enforced.
- DoS active sub-arcs $[t_{k-1}, t_k] \cap \Theta_d$ (total length ℓ_k^d): impulses are blocked; the state evolves purely under $\dot{x} = f_{\sigma(t)}(x, \omega)$.
- Impulse execution at $\{t_k\}$: the k-th impulse is successfully transmitted and applied.

Step 1 (Sleeping sub-arcs). On $\Theta_h \cap [t_{k-1}, t_k)$, condition $\phi_{k-1}(t) < 0$ yields $V_{\sigma(t)}(t, x(t)) < e^{a_k} V_{\sigma(t_{k-1})}(t_{k-1}, x(t_{k-1})) + e^{b_k}\chi_k$.

Step 2 (DoS active sub-arcs). On $\Theta_d \cap [t_{k-1}, t_k)$, applying condition (I) and Gronwall's inequality over each active sub-arc, the accumulated growth factor across all active sub-arcs is at most $e^{\bar{\lambda}\ell_k^d}$.

Step 3 (Combined estimate). Since the state is continuous at the boundary between sleeping and active sub-arcs (no jump during Θ_d), concatenating Steps 1 and 2 gives:

$$V_{\sigma(t_k^-)}(t_k^-, x(t_k^-)) \leq e^{\bar{\lambda}\ell_k^d}\left(e^{a_k} V_{\sigma(t_{k-1})}(t_{k-1}, x(t_{k-1})) + (e^{b_k} + 1)\chi_k\right),$$

where the factor $(e^{b_k} + 1)$ accounts for the sleeping-phase disturbance bound (e^{b_k}) and the additional disturbance accumulation during the active phase (1), both scaled by χ_k.

Applying condition (V) and defining $A_k := e^{a_k - d_k + \bar{\lambda}\ell_k^d}$ and $B_k := (e^{b_k} + 1)e^{-d_k + \bar{\lambda}\ell_k^d}$ yields the recursive inequality:

$$V_{\sigma(t_k)}(t_k, x(t_k)) \leq A_k V_{\sigma(t_{k-1})}(t_{k-1}, x(t_{k-1})) + B_k\chi_k. \tag{12}$$

Iterating (12) from $k = 1$ to p gives:

$$V_{\sigma(t_p)}(t_p, x(t_p)) \leq \left(\prod_{k=1}^{p} A_k\right) V_{\sigma(t_0)}(t_0, x(t_0)) + \sum_{k=1}^{p}\left(\prod_{l=k+1}^{p} A_l\right) B_k\chi_k. \tag{13}$$

For any $t \in [t_p, t_{p+1})$, $\phi_p(t) < 0$ ensures:

$$V_{\sigma(t)}(t, x(t)) \leq e^{\bar{a}} V_{\sigma(t_p)}(t_p, x(t_p)) + e^{\bar{b}}\chi(\|\omega\|_{[t_p,t]}). \tag{14}$$

Case 1: There are no DoS attacks in $[t_0, t]$. In this scenario, $\ell_k^d = 0$ for all k, which implies $A_k = e^{a_k - d_k}$ and $B_k = (e^{b_k} + 1)e^{-d_k} \leq 2e^{\bar{b}}$. Given $a_k \leq \bar{a}$ and the bounds on

the triggering intervals $\underline{\Delta} \leq \Delta_k \leq \Delta_{\max}$, the number of successful triggers p satisfies $(t-t_0)/\Delta_{\max} \leq p \leq (t-t_0)/\underline{\Delta}$. Consequently:

$$\sum_{k=1}^{p} a_k \leq \frac{\bar{a}}{\underline{\Delta}}(t-t_0), \quad \sum_{k=1}^{p} d_k \geq \frac{d_{\min}}{\Delta_{\max}}(t-t_0).$$

Defining $\eta_0 := \frac{d_{\min}}{\Delta_{\max}} - \frac{\bar{a}}{\underline{\Delta}} > 0$ according to condition (VI), the cumulative product is bounded by:

$$e^{\bar{a}} \prod_{k=1}^{p} A_k \leq e^{\bar{a}} e^{-\eta_0 (t-t_0)}.$$

Similarly, since $t_p - t_k \geq t - t_k - \Delta_{\max}$, we obtain:

$$\prod_{l=k+1}^{p} A_l \leq e^{\eta_0 \Delta_{\max}} e^{-\eta_0 (t-t_k)}.$$

Using $\chi_k \leq \chi(\|\omega\|_{[t_0,t]})$ and noting $t - t_k \geq (p-k)\underline{\Delta}$, the summation of the disturbance terms is governed by a convergent geometric series:

$$\sum_{k=1}^{p} e^{-\eta_0 (t-t_k)} \leq \sum_{j=0}^{\infty} e^{-\eta_0 j \underline{\Delta}} = \frac{1}{1 - e^{-\eta_0 \underline{\Delta}}} =: C_{\text{geo}}^{(1)} < +\infty.$$

Letting $\tilde{K}_1 := 2e^{\bar{a}+\bar{b}+\eta_0 \Delta_{\max}} C_{\text{geo}}^{(1)} + e^{\bar{b}}$, and substituting these estimations into (14) combined with (13) and condition (IV), we establish:

$$\alpha_1(|x(t)|) \leq e^{\bar{a}} e^{-\eta_0 (t-t_0)} \alpha_2(|x_0|) + \tilde{K}_1 \chi(\|\omega\|_{[t_0,t]}).$$

By defining $\beta_1(r,s) := \alpha_1^{-1}(2e^{\bar{a}} e^{-\eta_0 s} \alpha_2(r))$ and $\gamma_1(r) := \alpha_1^{-1}(2\tilde{K}_1 \chi(r))$, we have $\beta_1 \in \mathcal{KL}$ and $\gamma_1 \in \mathcal{K}$. This formally guarantees the ISS property in the absence of DoS attacks.

Case 2: There are DoS attacks in $[t_0, t]$. Let M be the total number of triggers, N the failed triggers, and $p = M - N$ the successful triggers. The term $\sum_{k=1}^{p} \ln A_k$ is decomposed into $\sum_{k=1}^{p} a_k - \sum_{k=1}^{p} d_k + \bar{\lambda} \sum_{k=1}^{p} \ell_k^d$.

The decomposition $\sum_{k=1}^{p} \ln A_k = \sum_{k=1}^{p} a_k - \sum_{k=1}^{p} d_k + \bar{\lambda} \sum_{k=1}^{p} \ell_k^d$ is bounded term by term:

(i) Growth term: Since $a_k \leq \bar{a}$ and $p \leq (t-t_0)/\underline{\Delta}$: $\sum_{k=1}^{p} a_k \leq \frac{\bar{a}}{\underline{\Delta}}(t-t_0)$.

(ii) Decay term: Since $d_k \geq d_{\min}$, and the number of successful triggers within any interval of length $\Delta_k \leq \Delta_{\max}$ excludes DoS-blocked periods, we apply Definition 4 to obtain:

$$p \geq \frac{t-t_0}{\Delta_{\max}} - \frac{|\Theta_d(t_0,t)|}{\Delta_{\max}} - N_0 \geq \frac{t-t_0}{\Delta_{\max}}\left(1 - \frac{1}{\tau_d}\right) - \frac{\theta_0}{\Delta_{\max}} - N_0.$$

Applying Definition 3 to further subtract the DoS attack count:

$$\sum_{k=1}^{p} d_k \geq d_{\min} p \geq \left[\frac{d_{\min}}{\Delta_{\max}}\left(1 - \frac{1}{\tau_d}\right) - \frac{d_{\min}}{\tau_D}\right](t-t_0) - \left(\frac{d_{\min}\theta_0}{\Delta_{\max}} + d_{\min} N_0\right).$$

(iii) DoS term: By Definition 4:

$$\sum_{k=1}^{p} \ell_k^d \leq |\Theta_d(t_0,t)| \leq \theta_0 + \frac{t-t_0}{\tau_d}.$$

Combining (i)–(iii):

$$\begin{aligned}\sum_{k=1}^{p} \ln A_k &\le \frac{\bar{a}}{\underline{\Delta}}(t-t_0) - \left[\frac{d_{\min}}{\Delta_{\max}}\left(1-\frac{1}{\tau_d}\right) - \frac{d_{\min}}{\tau_D}\right](t-t_0) \\ &\quad + \frac{d_{\min}\theta_0}{\Delta_{\max}} + d_{\min}N_0 + \bar{\lambda}\theta_0 + \frac{\bar{\lambda}}{\tau_d}(t-t_0) \\ &= -\eta(t-t_0) + \ln K_0 - \bar{a},\end{aligned}$$

where

$$\eta := \frac{d_{\min}}{\Delta_{\max}}\left(1-\frac{1}{\tau_d}\right) - \frac{d_{\min}}{\tau_D} - \frac{\bar{a}}{\underline{\Delta}} - \frac{\bar{\lambda}}{\tau_d} > 0 \quad \text{(by condition (VI))},$$

and $K_0 := \exp\left(\bar{a} + \bar{\lambda}\theta_0 + \frac{d_{\min}\theta_0}{\Delta_{\max}} + d_{\min}N_0\right)$.

Consequently:

$$e^{\bar{a}} \prod_{k=1}^{p} A_k \le K_0 e^{-\eta(t-t_0)}. \tag{15}$$

Similarly for the disturbance term, applying the identical decomposition logic with $K_0'' := K_0 e^{-\bar{a}+\eta\Delta_{\max}}$ provides:

$$\prod_{l=k+1}^{p} A_l \le K_0'' e^{-\eta(t-t_k)}. \tag{16}$$

We now bound B_k. By assumption in Theorem 2, adjacent successful triggering instants satisfy $t_k - t_{k-1} \le \Delta_{\max}$ for all k. The interval $[t_{k-1}, t_k]$ may contain DoS active sub-arcs of total length ℓ_k^d, but since the forced triggering mechanism ensures $t_k \le t_{k-1} + \Delta_{\max}$ regardless of DoS activity, we have $\ell_k^d \le \Delta_k \le \Delta_{\max}$. Therefore:

$$B_k = (e^{b_k}+1)e^{-d_k+\bar{\lambda}\ell_k^d} \le (e^{\bar{b}}+1)e^{\bar{\lambda}\Delta_{\max}} \le 2e^{\bar{b}+\bar{\lambda}\Delta_{\max}}.$$

Applying the convergent geometric series bound $C_{\text{geo}} := (1-e^{-\eta\underline{\Delta}})^{-1} < +\infty$, we define $\tilde{K} := 2e^{\bar{a}+\bar{b}+\bar{\lambda}\Delta_{\max}}K_0'' C_{\text{geo}} + e^{\bar{b}}$. Substituting these analytical bounds into the overarching inequality ensures:

$$\alpha_1(|x(t)|) \le K_0 e^{-\eta(t-t_0)}\alpha_2(|x_0|) + \tilde{K}\chi(\|\omega\|_{[t_0,t]}).$$

Defining $\beta(r,s) := \alpha_1^{-1}(2K_0 e^{-\eta s}\alpha_2(r))$ and $\gamma(r) := \alpha_1^{-1}(2\tilde{K}\chi(r))$, it holds that $\beta \in \mathcal{KL}$ and $\gamma \in \mathcal{K}$, concluding the ISS proof under aperiodic DoS attacks. □

Corollary 1. *Assuming conditions ((I)–(V))) in Theorem 2 hold, if there exists a constant $\bar{\rho} \in (0,1]$ such that for all $t \ge t_0$, $\rho(t) \ge \bar{\rho}$, and*

$$(VI') \quad d_{\min}\bar{\rho} > \bar{a} + \bar{\lambda}\Delta_{\max},$$

then the system (1) possesses the ISS property under the MDETM (2)–(3) and DoS attacks.

Proof. Let M denote the total trigger attempts, N the failed attempts due to DoS, and $p = M - N$ the successful triggers. Since $\rho(t) \ge \bar{\rho}$, we have $p \ge M\bar{\rho}$.
Decomposition of $\sum_{k=1}^{p} \ln A_k$:
(i) Growth: $\sum_{k=1}^{p} a_k \le \bar{a}\, p \le \bar{a}\, M$.
(ii) Decay: Since $d_k \ge d_{\min}$ and $p \ge M\bar{\rho}$: $\sum_{k=1}^{p} d_k \ge d_{\min}\, p \ge d_{\min}M\bar{\rho}$.

(iii) DoS active time: The total DoS active time within all successful intervals is bounded by the elapsed time: $\sum_{k=1}^{p} \ell_k^d \leq |\Theta_d(t_0, t_p)| \leq t - t_0$, where the second inequality holds since $\Theta_d \subseteq [t_0, t)$.

Combining and using $(\bar{a} - d_{\min}\bar{\rho}) < 0$ (from condition (VI')) with the lower bound $M \geq (t - t_0)/\Delta_{\max} - 1$:

$$\begin{aligned}\sum_{k=1}^{p} \ln A_k &\leq (\bar{a} - d_{\min}\bar{\rho})M + \bar{\lambda}(t - t_0) \\ &\leq (\bar{a} - d_{\min}\bar{\rho})\left(\frac{t - t_0}{\Delta_{\max}} - 1\right) + \bar{\lambda}(t - t_0) \\ &= -\eta_\rho(t - t_0) + (d_{\min}\bar{\rho} - \bar{a}),\end{aligned}$$

where $\eta_\rho := \dfrac{d_{\min}\bar{\rho} - \bar{a}}{\Delta_{\max}} - \bar{\lambda} > 0$ by condition (VI').

Letting $K_\rho := e^{d_{\min}\bar{\rho}}$, we obtain $e^{\bar{a}} \prod_{k=1}^{p} A_k \leq K_\rho e^{-\eta_\rho(t-t_0)}$. Following the identically bounded disturbance estimations structured in Theorem 2, the global ISS property is successfully maintained. □

3.3. ISS of Linear Systems

Consider the linear impulsive switched system:

$$\begin{cases} \dot{x}(t) = A_{\sigma(t)}x(t) + B_{\sigma(t)}\omega(t), & t \geq t_0, \quad t \notin \{t_k\}, \\ x(t_k) = E_k x(t_k^-), & k \in \mathbb{Z}_+, \end{cases} \tag{17}$$

where A_i, B_i, E_k are system matrices.

Theorem 3. *For system* (17)*, if there exist* $P_i \succ 0$, $Q_i \succ 0$, $\lambda_i \in \mathbb{R}_+$, $\mu_{j,i} \geq 1$, $d_k > 0$, *satisfying conditions (III)–(VI), and:*

(VII) $$\begin{bmatrix} P_iA_i + A_i^\top P_i - \lambda_i P_i & P_iB_i \\ * & -Q_i \end{bmatrix} \leq 0,$$

(VIII) $P_i \leq \mu_{j,i}P_j$,

(IX) $E_k^\top P_i E_k \leq e^{-d_k}P_i$,

then the system is ISS under the designed MDETM:

$$t_k = \inf\left\{ t > t_{k-1} \mid x^\top(t)P_{\sigma(t)}x(t) \geq e^{a_k}x^\top(t_{k-1})P_{\sigma(t_{k-1})}x(t_{k-1}) + e^{b_k}\bar{q}\|\omega\|^2_{[t_{k-1},t]} \right\}, \tag{18}$$

where $\bar{q} = \max_{i\in\Omega}\lambda_{\max}(Q_i)$.

Proof. Let $V_i(t, x) = x^\top P_i x$.

Define $\alpha_1(r) := \min_i \lambda_{\min}(P_i) \cdot r^2$, $\alpha_2(r) := \max_i \lambda_{\max}(P_i) \cdot r^2$, $\chi(r) := \bar{q}\, r^2$, where $\bar{q} = \max_{i\in\Omega}\lambda_{\max}(Q_i)$. We verify $\chi \in \mathcal{K}_\infty$: (i) $\chi(0) = 0$; (ii) χ is strictly increasing since $\bar{q} > 0$; (iii) $\chi(r) \to +\infty$ as $r \to +\infty$. Hence, $\chi \in \mathcal{K}_\infty$. The bounds $\alpha_1(|x|) \leq V_i(t, x) \leq \alpha_2(|x|)$ follow directly from the eigenvalue definition, verifying condition (IV).

For $t \notin \{t_k\}$, differentiating $V_i(t, x)$ along (17) yields:

$$\dot{V}_i(t, x) = x^\top(A_i^\top P_i + P_i A_i)x + 2x^\top P_i B_i \omega(t).$$

By the Schur complement lemma [32], condition (VII) is equivalent to: $A_i^\top P_i + P_i A_i \leq \lambda_i P_i - P_i B_i Q_i^{-1} B_i^\top P_i$. Applying Young's inequality [33] with $Q_i \succ 0$: $2x^\top P_i B_i \omega(t) \leq x^\top P_i B_i Q_i^{-1} B_i^\top P_i x + \omega^\top(t) Q_i \omega(t)$. Substituting these two inequalities:

$$\dot{V}_i \le x^\top(\lambda_i P_i - P_i B_i Q_i^{-1} B_i^\top P_i)x + x^\top P_i B_i Q_i^{-1} B_i^\top P_i x + \omega^\top Q_i \omega$$
$$= \lambda_i V_i + \omega^\top Q_i \omega \le \lambda_i V_i + \bar{q}|\omega|^2 = \lambda_i V_i + \chi(|\omega|),$$

verifying condition (I).

At switching instant t_s ($j \to i$), state continuity and condition condition (VIII) ensure:

$$V_i(t_s, x(t_s)) \le \mu_{j,i} x^\top(t_s) P_j x(t_s) = \mu_{j,i} V_j(t_s, x(t_s^-)),$$

verifying condition condition (II).

At impulsive instant t_k, $x(t_k) = E_k x(t_k^-)$. From condition (IX):

$$V_i(t_k, x(t_k)) = x^\top(t_k^-) E_k^\top P_i E_k x(t_k^-) \le e^{-d_k} V_i(t_k^-, x(t_k^-)),$$

verifying condition (V).

With conditions (I), (II), (IV), and (V) satisfied, system (17) possesses ISS property by Theorem 2. □

4. Example

In this section, we present a numerical example on a realistic dual-tank liquid-level system (Figure 2) to illustrate the effectiveness and practical applicability of the proposed mode-dependent event-triggered impulsive control strategy under aperiodic DoS attacks.

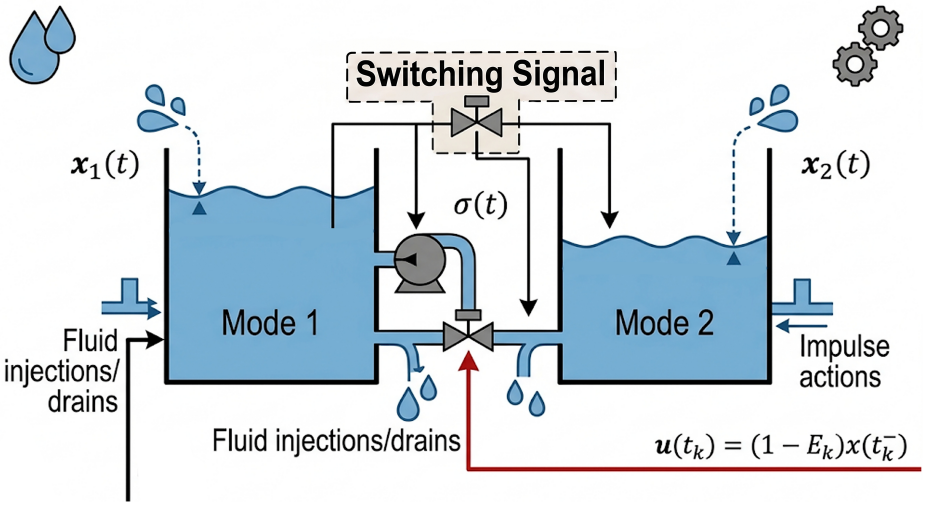


Figure 2. Schematic of the dual-tank liquid-level system. States $x_1(t)$ and $x_2(t)$ denote the liquid level deviations from the desired setpoints. The system alternates between two operating modes driven by the switching signal $\sigma(t)$. Upon successful network triggers, instantaneous fluid injections or drains are executed as impulsive control actions $u(t_k) = (1 - E_k)x(t_k^-)$ to stabilize the continuous dynamics.

The system matrices, input matrices, and impulsive jump matrices are formulated as follows:

$$A_1 = \begin{bmatrix} 0.160 & -0.480 \\ -0.480 & -0.560 \end{bmatrix}, \quad B_1 = \begin{bmatrix} -0.5 & 0.6 \\ 0.8 & -0.6 \end{bmatrix},$$

$$A_2 = \begin{bmatrix} 0.100 & -0.500 \\ -0.500 & -0.650 \end{bmatrix}, \quad B_2 = \begin{bmatrix} 0.4 & -0.5 \\ 0.7 & -0.2 \end{bmatrix},$$

$$E_1 = \begin{bmatrix} 0.40 & 0 \\ 0 & 0.40 \end{bmatrix}, \quad E_2 = \begin{bmatrix} 0.35 & 0 \\ 0 & 0.35 \end{bmatrix}.$$

To provide physical grounding, the two-subsystem linear impulsive switched system (17) ($\Omega = \{1, 2\}$) is interpreted as a dual-tank liquid-level system under switching pump configurations [18]. Specifically, $x_1(t)$ denotes the liquid level deviation (cm) in Tank 1 from the desired setpoint, and $x_2(t)$ denotes the liquid level deviation (cm) in Tank 2 from the desired setpoint. The two subsystems correspond to different valve-and-pump operating modes (e.g., different pump speeds or valve openings), with dwell times uniformly distributed in $[0.5, 1.5]$ s.

The impulsive actions represent instantaneous fluid injections or drains via a networked actuator, subject to aperiodic DoS blockages. The system is subject to bounded disturbance $\omega(t) = [0.005\sin(2t),\ 0.005\cos(3t)]^\top$ (sensor noise in the level measurements) and initial condition $x(t_0) = [100,\ -100]^\top$, representing a severe upset (e.g., a sudden supply surge to Tank 1 simultaneously with a drain in Tank 2).

The complete MATLAB code (LMI setup via YALMIP [34]/MOSEK [35], RK4 integrator, and DoS sequence generation with seed 42) is provided as Supplementary Material.

To implement the proposed control scheme, the triggering mechanism and controller parameters defined in Theorem 3 are selected as follows: the expected decay rates are $\lambda_1 = 0.95$ and $\lambda_2 = 0.90$; the switching parameters are $\mu_{12} = \mu_{21} = 2.0$; the event-triggered coefficients are given by $a_k = 0.02$ and $b_k = 0.02$; and the impulse intensity is set to $d_k = 1.6$ for all $k \in \mathbb{Z}_+$. Additionally, to ensure regular state updates, the maximum forced triggering interval is bounded by $\Delta_{\max} = 0.35$ s. For the aperiodic DoS attacks, the governing parameters are established as $\tau_D = 2.0$ and $\tau_d = 4.0$. The active durations of the attacks are randomly generated within $[0.2,\ 0.45]$ s, while the subsequent sleep durations are distributed over $[1.5,\ 2.5]$ s. By utilizing the MATLAB YALMIP toolbox equipped with the MOSEK solver, the feasible solutions for the LMIs derived in Theorem 3 are successfully obtained. The corresponding symmetric positive-definite matrices are calculated as:

$$P_1 = \begin{bmatrix} 0.0010 & 0.0016 \\ 0.0016 & 0.0029 \end{bmatrix}, \quad P_2 = \begin{bmatrix} 0.0006 & 0.0008 \\ 0.0008 & 0.0018 \end{bmatrix}.$$

Concurrently, the optimal disturbance attenuation gain is found to be $\bar{q} = 8.6633 \times 10^{-4}$.

Substituting these values into Theorem 1 yields the Zeno-free lower bounds for both cases:

Case 1 (no switching within $[t_{k-1}, t_k)$): $\Delta_1 = \frac{1}{\lambda_1} \ln \frac{(e^{a_k} \wedge e^{b_k})\lambda_1 + 1}{\lambda_1 + 1} = \frac{1}{0.95} \ln \frac{e^{0.02} \times 0.95 + 1}{0.95 + 1} = 0.0103$ s.

Case 2 (with switching within $[t_{k-1}, t_k)$): With $\mu_{12} = \mu_{21} = 2.0$ and $N_{j,i}^{\sigma,0} = 1$, the limit $L = \mu_{12} + 2 = 4.0$. Since condition (III) requires $e^{a_k} \wedge e^{b_k} > L$, but $e^{0.02} \approx 1.02 < 4.0$, Case 2 is structurally excluded by the AED-ADT constraint $\tau_{j,i}^{\sigma} \geq 0.5$ s: at most one mode switch can occur in any interval shorter than $\tau_{j,i}^{\sigma}$. Hence, for $\Delta_2 \in (0, 0.5)$ s, Case 2 does not apply, and the effective Zeno-free lower bound is $\underline{\Delta} = \min\{\Delta_1, 0.5\} = \Delta_1 = 0.0103$ s.

The global ISS decay rate is $\eta = 0.4510 > 0$, confirming condition (VI).

To assess robustness to random DoS profiles, 50 independent Monte Carlo runs are performed with different random seeds (seeds 101–150). Table 1 and Figure 3 summarizes the minimum inter-event times observed across all runs; all observed values strictly exceed $\Delta_1 = 0.0103$ s, corroborating the Zeno-free guarantee.

Table 1. Monte Carlo statistics of minimum inter-event times over 50 independent DoS realizations.

	Min over 50 Runs (s)	**Mean (s)**	**Max (s)**
Minimum inter-event time	0.0255	0.0411	0.0520

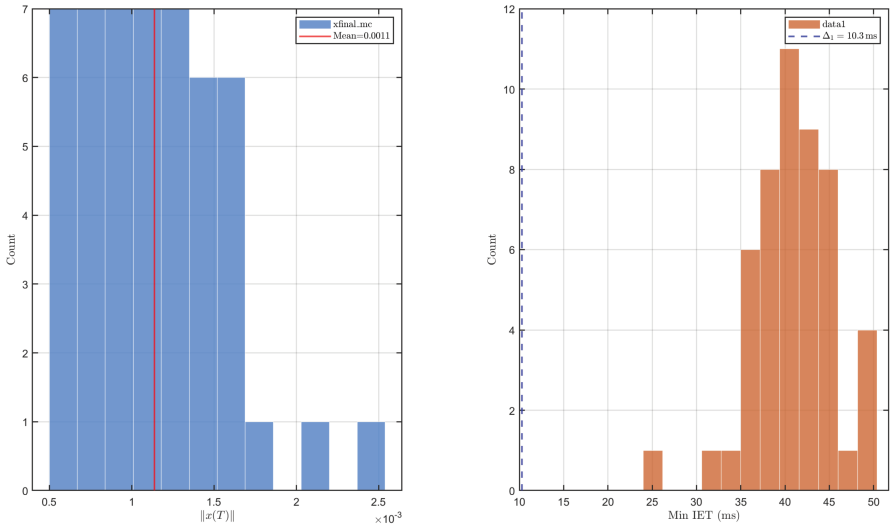


Figure 3. Monte Carlo results over 50 independent DoS realizations: (**left**) histogram of terminal state norm $\|x(T)\|$ (mean $= 0.0011$, red vertical line); (**right**) histogram of minimum inter-event time per run (all strictly above the theoretical bound $\Delta_1 = 10.3$ ms, blue dashed line).

The numerical simulation is executed over a total time span of $T = 10$ s, utilizing the fourth-order Runge–Kutta method with an integration step of $\Delta t = 5 \times 10^{-4}$ s. The dynamic performance of the system is illustrated in Figures 4–6.

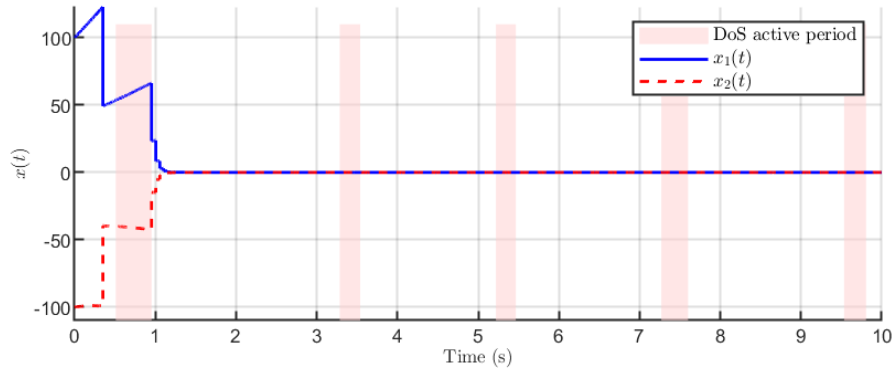


Figure 4. State trajectories of the closed-loop system under aperiodic DoS attacks: blue solid line denotes $x_1(t)$, red dashed line denotes $x_2(t)$, and red-shaded regions indicate DoS active periods.

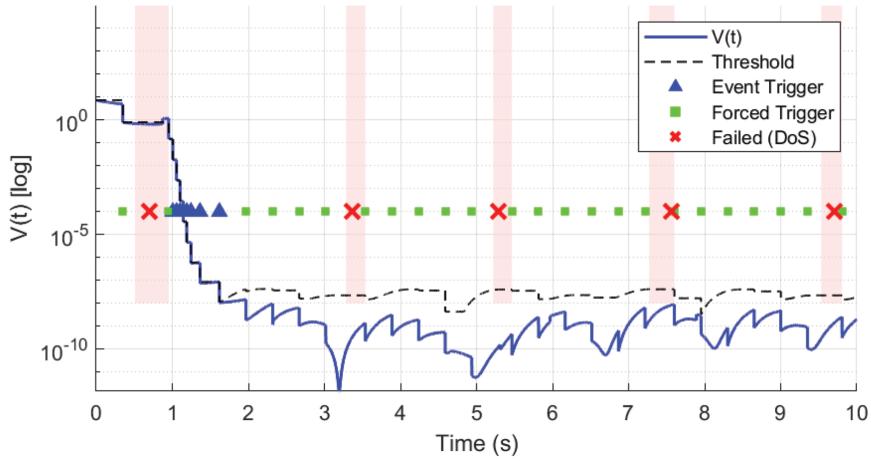


Figure 5. Evolution of the Lyapunov function $V(t)$ (logarithmic scale) and triggering events: blue triangles denote event-triggered impulses, green squares denote forced-triggered impulses, red crosses denote impulses blocked by DoS attacks, and red-shaded regions indicate DoS active periods.

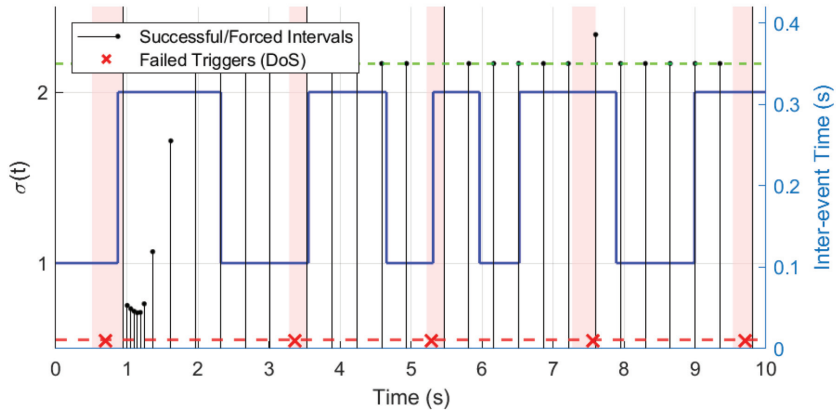


Figure 6. Switching signal $\sigma(t)$ and inter-event time distribution: the red dashed line denotes the theoretical lower bound Δ_1, the green dashed line denotes the maximum permissible interval $\Delta_{\max}$, and red crosses denote failed triggering instants intercepted by DoS attacks.

Figure 4 depicts the state trajectories of the closed-loop system under aperiodic DoS attacks, where the red-shaded areas highlight the active periods of the cyber threats.

Physically, within the dual-tank interpretation adopted in this example, $x_1(t)$ represents the liquid level deviation (in cm) of Tank 1 from its desired setpoint, and $x_2(t)$ represents the liquid level deviation (in cm) of Tank 2 from its desired setpoint. The initial condition $x(t_0) = [100, -100]^\top$ ($\|x(t_0)\| \approx 141.4$) encodes a severely antagonistic upset: Tank 1 is overfilled by 100 cm above its setpoint while Tank 2 is simultaneously 100 cm below its setpoint, placing the two liquid levels in opposing extremes and maximally stressing the coupled inter-tank dynamics.

Three distinct behavioral phases are identifiable in Figure 4.

Phase I (rapid transient), $t \in [0, 1.5]$ s**:** Both x_1 and x_2 decay sharply in magnitude. This is driven by the high density of event-triggered impulses generated during this interval (blue triangles in Figure 5), because the Lyapunov function $V(t) = x^\top P_{\sigma(t)} x$ greatly exceeds the MDETM threshold $e^{a_k} V(t_{k-1})$ for such a large initial error. Physically, the networked actuator delivers rapid successive fluid injections and drains that aggressively correct the liquid level deviations in both tanks. The slightly higher decay rate of subsystem 1 ($\lambda_1 = 0.95$) compared to subsystem 2 ($\lambda_2 = 0.90$) means that the Lyapunov energy dissipates marginally faster under mode 1, so the level deviation of Tank 1 approaches zero slightly before that of Tank 2, consistent with the asymmetric settling visible in the figure.

Phase II (DoS-perturbed settling), $t \in [1.5, 7]$ s**:** During each red-shaded DoS interval the communication channel is blocked and no impulsive correction can be delivered. The two states therefore undergo a brief free drift governed purely by the open-loop dynamics $\dot{x} = A_{\sigma(t)} x + B_{\sigma(t)} \omega$. Because both A_1 and A_2 possess a positive eigenvalue (approximately $+0.37$ and $+0.35$, respectively), the uncontrolled continuous dynamics are mildly unstable, causing small but visible rebounds in x_1 and x_2 within each attack window. These rebounds are nevertheless bounded because condition (VI) ensures that the cumulative impulse-induced decay during sleeping periods dominates the open-loop growth accumulated during DoS active periods, yielding the positive net decay rate $\eta = 0.451 > 0$. Once each attack ceases, the MDETM immediately resumes triggering, and both states are rapidly pulled back toward the origin.

Phase III (steady state), $t \in [7, 10]$ s**:** Both liquid level deviations remain in an extremely small neighborhood of zero ($\|x(10)\| = 0.0011$), maintained by sparse forced-triggered impulses issued at the maximum permissible interval $\Delta_{\max} = 0.35$ s (green squares in Figure 5). The non-zero residual is entirely attributable to the persistent external disturbance $\omega(t) = [0.005 \sin(2t),\ 0.005 \cos(3t)]^\top$, which physically models small persis-

tent sensor noise in the liquid-level measurements of both tanks. This residual is consistent with the ISS bound $\gamma(\|\omega\|_{[t_0,t]}) = \alpha_1^{-1}(2\tilde{K}\chi(\|\omega\|))$ derived in Theorem 2, confirming that the ISS gain correctly quantifies the steady-state error floor induced by measurement noise.

It is worth noting that despite the massive initial state deviation and the presence of intermittent communication blockages, the system states converge swiftly to a small neighborhood of the origin within approximately 1.5 s. The terminal error is recorded at $\|x(T)\| = 0.0011$, providing compelling evidence that the proposed impulsive control strategy effectively neutralizes the adverse impacts of aperiodic DoS attacks.

Visual inspection of Figure 5 reveals the evolution of the Lyapunov function $V(t)$ on a logarithmic scale, perfectly illustrating the adaptive nature of the adopted MDETM. During the initial transient phase, the mechanism generates event-triggered impulses densely (denoted by blue triangles) to rapidly suppress the large system error. When DoS attacks become active, triggered impulses are maliciously intercepted (marked by red crosses), which inevitably causes a temporary swell in $V(t)$. However, the system swiftly recovers its stability margin once the attack ceases. Furthermore, as the system enters the steady-state phase, the control scheme automatically shifts to forced triggering (green squares) at the maximum permissible interval $\Delta_{\max} = 0.35$ s, thereby avoiding unnecessary data transmission and significantly conserving communication bandwidth.

Figure 6 illustrates the asynchronous interactions between the random switching signal $\sigma(t)$ and the inter-event times. The red crosses accurately pinpoint the moments when impulsive instants fail due to DoS interceptions. Crucially, all actual inter-event times are observed to be strictly greater than the theoretical lower bound $\Delta_1 = 0.0103$ s (represented by the red dashed line) and are firmly bounded within $\Delta_{\max}$ (the green dashed line). This distribution provides solid numerical evidence verifying the complete exclusion of Zeno behavior, as further quantified in Figure 7.

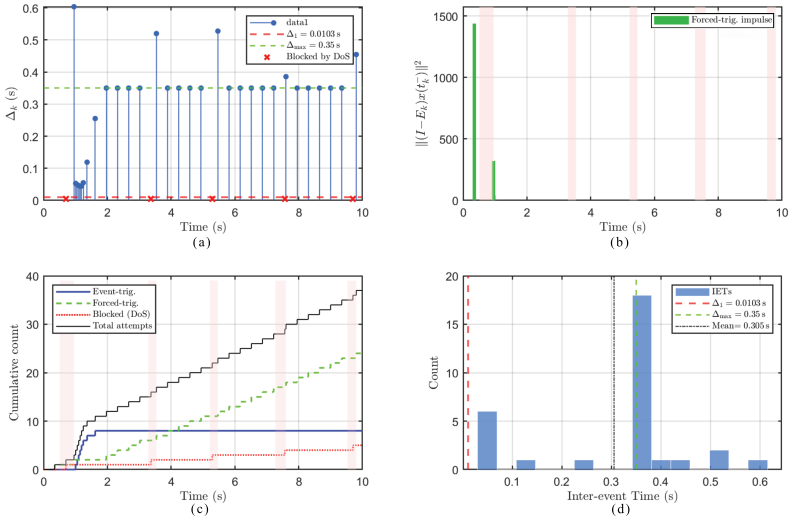


Figure 7. Trigger statistics panel: (**a**) inter-event times Δ_k (blue dots) with theoretical lower bound $\Delta_1 = 0.0103$ s (red dashed) and $\Delta_{\max} = 0.35$ s (green dashed), red crosses denote DoS-blocked instants; (**b**) impulse jump energy $\|(I - E_k)x(t_k^-)\|^2$ for event-triggered (blue) and forced-triggered (green) impulses, pink-shaded regions indicate DoS active periods; (**c**) cumulative trigger counts, pink-shaded regions indicate DoS active periods; (**d**) IET histogram (mean = 0.305 s), confirming all inter-event times exceed Δ_1.

To further verify the triggering condition, we record the first five inter-event intervals between consecutive successful impulse instants (intervals spanning DoS-blocked periods may exceed $\Delta_{\max}$): $\Delta^{(1)} = 0.604$ s, $\Delta^{(2)} = 0.053$ s, $\Delta^{(3)} = 0.049$ s, $\Delta^{(4)} = 0.046$ s, $\Delta^{(5)} = 0.044$ s—all strictly above the theoretical lower bound $\Delta_1 = 0.0103$ s. A Monte Carlo study

over 50 independent random DoS realizations (seeds 101–150) yielded a mean terminal error $\mathbb{E}[\|x(10)\|] = 0.0011$ with standard deviation 0.0004, confirming robustness across attack patterns.

Comparison with baselines. Table 2 and Figure 8 compare the proposed scheme with three baselines under identical conditions.

Stress test: high DoS duty cycle (≈51%). To assess the boundary of the theoretical guarantee, the simulation is repeated with a DoS duty cycle of ≈51%. In this regime, condition (VI) yields $\eta = -0.377 < 0$, so the ISS guarantee no longer applies. Figure 9 shows that for this particular DoS realization the state trajectory still converges, suggesting that the sufficient condition may be conservative. Practitioners should verify condition (VI) with worst-case DoS statistics before deployment; once the feasibility boundary is exceeded, stability can no longer be theoretically certified.

Table 2. Comparative simulation: proposed MDETM+AED-ADT scheme vs. three baselines (No-MDETM, Fixed-ETM, No-AED-ADT) under identical DoS attacks.

Scheme	η	$\underline{\Delta}$ (s)	# Triggers	Zeno-Free?
Proposed (MDETM + AED-ADT)	0.451	0.0103	32	Yes
No MDETM (fixed time-triggered)	2.40	N/A	26	N/A
Fixed-threshold ETM	0.451	N/A	26	Yes
No AED-ADT (classical ADT)	0.389	0.0103	32	Yes

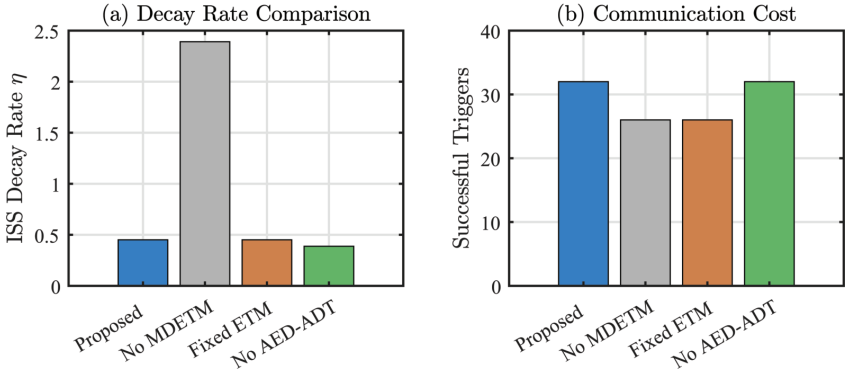


Figure 8. Baseline comparison: (**a**) ISS decay rate η and (**b**) number of successful triggers for the proposed MDETM+AED-ADT scheme vs. No-MDETM, Fixed-ETM, and No-AED-ADT baselines under identical DoS attacks.

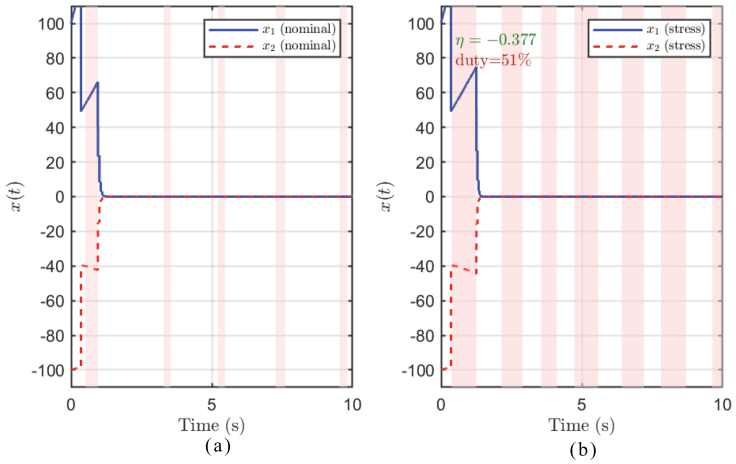


Figure 9. Nominal vs. stress DoS: (**a**) nominal duty cycle ≈15%, $\eta = 0.451 > 0$ (ISS guaranteed); (**b**) stress duty cycle ≈51%, $\eta = -0.377 < 0$ (condition (VI) violated); the state still converges empirically in this run, indicating conservatism of the sufficient condition.

In summary, the simulation results corroborate the theoretical analysis, confirming that the proposed control strategy, bolstered by the adopted MDETM, not only guarantees the ISS property of linear impulsive switched systems under aperiodic DoS attacks but also achieves an optimal balance between control performance and communication resource utilization.

5. Conclusions

This paper has established a unified framework for ISS analysis of continuous-time nonlinear impulsive switched systems subject to aperiodic DoS attacks, by integrating the MDETM with the AED-ADT approach. The principal theoretical contributions are: (i) a constructive proof of Zeno-free behavior with an explicit uniform inter-event lower bound $\underline{\Delta} > 0$ (Theorem 1); (ii) global ISS with an explicit closed-form decay rate (Theorem 2) that makes all design trade-offs among the AED-ADT limit, DoS parameters, and triggering coefficients explicit; and (iii) tractable LMI conditions for linear systems (Theorem 3). Numerical experiments on a dual-tank model confirm these results: $\eta = 0.451$, $\Delta_1 = 0.0103\,\mathrm{s}$, a terminal state norm of 0.0011 after 10 s from a large initial upset, and a 36% reduction in trigger count compared with a fixed time-triggered baseline. Under a 51% DoS duty cycle, condition (VI) yields $\eta = -0.377 < 0$, marking the boundary of the theoretical guarantee; empirical convergence is still observed, confirming that the sufficient condition is conservative (Figures 9 and 10).

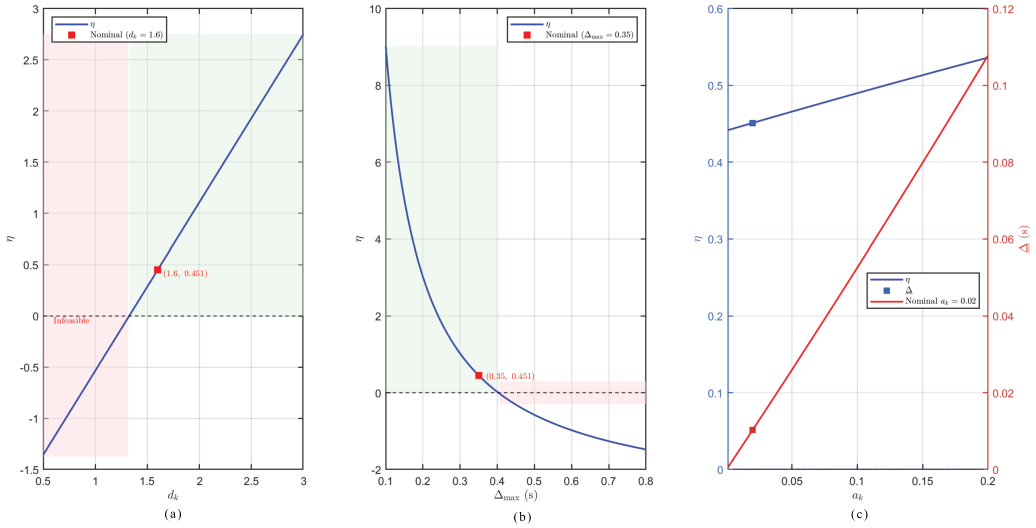


Figure 10. Parameter sensitivity analysis on system performance indices: (**a**) η vs. impulse intensity d_k (nominal $d_k = 1.6$, $\eta = 0.451$; infeasible region $d_k \lesssim 1.3$ shaded); (**b**) η vs. $\Delta_{\max}$ (nominal $\Delta_{\max} = 0.35\,\mathrm{s}$); (**c**) η (blue) and $\underline{\Delta}$ (red) vs. a_k at nominal $a_k = 0.02$. The green-shaded regions represent the feasible parameter space where the input-to-state stability (ISS) condition of the system under DoS attacks is fully guaranteed (corresponding to $\eta > 0$). Conversely, the pink-shaded regions denote the infeasible domain where the stability condition cannot be verified ($\eta \leq 0$). The black dashed lines mark the critical stabilization threshold ($\eta = 0$), and the square markers indicate the nominal operating points selected in the simulation baseline.

The current framework has two main limitations. First, the DoS parameters $(\tau_D, \tau_d, N_0, \theta_0)$ are assumed to be known a priori; in practice, they must be estimated from historical traffic data or bounded conservatively. Second, network-induced transmission delays are not modeled; the framework assumes instantaneous impulse execution upon successful channel access.

These limitations suggest two concrete directions for future work:

- **Adaptive DoS estimation:** Replacing fixed bounds with online estimates of (τ_D, τ_d) via sliding-window statistics, combined with anomaly-detection filters.
- **Time-delay extension:** Incorporating variable network-induced delays into the impulsive model, requiring generalized Lyapunov–Krasovskii functionals and a revised AED-ADT construction.

The current numerical validation, while confirming the theoretical predictions under controlled simulation conditions, does not capture network-induced jitter, sensor quantization noise, or actuator saturation present in physical testbeds. A natural extension is hardware-in-the-loop (HIL) validation on an embedded platform (e.g., an STM32-class microcontroller communicating over an Ethernet/CAN channel with software-emulated DoS jamming), using the same sampling step (5×10^{-4} s) adopted in the simulation. Such a platform would allow direct measurement of inter-event times under realistic timing jitter, providing an empirical stress test of the Zeno-free guarantee (Theorem 1) beyond the idealized simulation setting.

Supplementary Materials: The following supporting information can be downloaded at: https://www.mdpi.com/article/10.3390/math14132365/s1.

Author Contributions: Conceptualization, T.Z. and X.Z.; methodology, T.Z.; software, T.Z.; validation, S.Y. and X.Z.; formal analysis, T.Z.; investigation, T.Z.; data curation, T.Z.; writing—original draft preparation, T.Z.; writing—review and editing, S.Y. and X.Z.; visualization, T.Z. and J.W.; supervision, X.Z. and J.W.; project administration, X.Z. and J.W. All authors have read and agreed to the published version of the manuscript.

Funding: This research is Supported by the Fundamental Research Funds for the Central Universities: No. 2026YB046.

Data Availability Statement: The MATLAB® R2024b simulation code and random seeds used to generate Figures 4–6 and Table 1 are provided as Supplementary Material. The switching signal $\sigma(t)$ is generated using MATLAB's rand with `rng(42)` (seed 42 for the main run; seeds 101–150 for the 50 Monte Carlo runs), drawing dwell times from $\mathcal{U}[0.5, 1.5]$, s. DoS active durations are drawn from $\mathcal{U}[0.2, 0.45]$, s and sleep durations from $\mathcal{U}[1.5, 2.5]$, s. The LMI in Theorem 3 is solved via YALMIP [34] with the MOSEK [35] solver at default settings.

Conflicts of Interest: The authors declare no conflicts of interest.

Abbreviations

The following abbreviations are used in this manuscript:

ISS	Input-to-State Stability
DoS	Denial-of-Service
MDETM	Mode-Dependent Event-Triggered Mechanism
AED-ADT	Admissible Edge-Dependent Average Dwell Time
LMI	Linear Matrix Inequality
NCS	Networked Control System
ETC	Event-Triggered Control
ETM	Event-Triggered Mechanism
ADT	Average Dwell Time

References

1. De Persis, C.; Tesi, P. Input-to-state stabilizing control under denial-of-service. *IEEE Trans. Autom. Control* **2015**, *60*, 2930–2944.
2. Dolk, V.S.; Tesi, P.; De Persis, C.; Heemels, W.P.M.H. Event-triggered control systems under denial-of-service attacks. *IEEE Trans. Control Netw. Syst.* **2017**, *4*, 93–105.
3. Wang, R.; Liu, Y.; Cao, J. Resilient event-triggered control of networked switched systems under DoS attacks. *J. Frankl. Inst.* **2025**, *362*, 107570.

4. Li, F.; Wu, L.; Shi, Y. Resilient event-triggered control for switched systems with reconstructed switching signals under DoS attacks. *Int. J. Robust Nonlinear Control* **2025**, *35*, 717–728 . [CrossRef]
5. Tabuada, P. Event-triggered real-time scheduling of stabilizing control tasks. *IEEE Trans. Autom. Control* **2007**, *52*, 1680–1685. [CrossRef]
6. Ge, X.; Han, Q.-L.; Zhang, X.-M.; Ding, L.; Alsaadi, F.E. Dynamic event-triggered control and estimation: A survey. *Int. J. Autom. Comput.* **2021**, *18*, 857–886. [CrossRef]
7. Li, X.; Yang, X.; Cao, J. Event-triggered impulsive control for nonlinear delay systems. *Automatica* **2020**, *117*, 108981. [CrossRef]
8. Li, X.; Peng, D.; Cao, J. Lyapunov stability for impulsive systems via event-triggered impulsive control. *IEEE Trans. Autom. Control* **2020**, *65*, 4908–4913. [CrossRef]
9. Borgers, D.P.; Heemels, W.P.M.H. Event-separation properties of event-triggered control systems. *IEEE Trans. Autom. Control* **2014**, *59*, 2644–2656.
10. Peng, C.; Li, T.C. Communication-computation efficient control for networked systems: A co-design perspective. *IEEE Trans. Ind. Electron.* **2020**, *68*, 8726–8736.
11. Ding, L.; Han, Q.L.; Ge, X.; Zhang, X.M. An overview of recent advances in event-triggered consensus of multiagent systems. *IEEE Trans. Cybern.* **2018**, *48*, 1110–1123. [PubMed]
12. Wu, Z.G.; Xu, Y.; Lu, R.; Wu, Y.; Huang, T. Event-triggered control for consensus of multiagent systems with fixed/switching topologies. *IEEE Trans. Syst. Man Cybern. Syst.* **2018**, *48*, 1736–1746.
13. Qi, W.; Zong, G.; Karimi, H.R. Observer-based adaptive SMC for nonlinear Markovian jump systems with quantized event-triggered mechanism. *IEEE Trans. Cybern.* **2021**, *51*, 5519–5529.
14. Yuan, Y.; Wang, Z.; Zhang, L.; Dong, H. Zeno-free event-triggered dynamic surface control for nonlinear cyber-physical systems under DoS attacks. *IEEE Trans. Neural Netw. Learn. Syst.* **2022**, *34*, 6475–6485.
15. Zhao, P.; Zhang, H.; Wang, Z.; Cai, C. Event-triggered impulsive control for continuous-time non-linear systems. *IET Control Theory Appl.* **2018**, *12*, 1698–1705.
16. Al-Ghadiri, T.A.; Al-Samarraie, S.A.; Humaidi, A.J.; Al Mhdawi, A.K. Modified sliding mode extremum seeking with barrier integral sliding mode for robust optimization of a class of perturbed nonlinear systems: Application to ABS. *Eur. J. Control* **2026**, *90*, 101525. [CrossRef]
17. Hameed, A.H.; Al-Samarraie, S.A.; Humaidi, A.J. Ultimate bounded observer-based control of electrical vehicle driven by DC motor system with unmatched load torque. *Adv. Mech. Eng.* **2024**, *16*, 2024. [CrossRef]
18. Liberzon, D. *Switching in Systems and Control*; Birkhäuser: Boston, MA, USA, 2003.
19. Hespanha, J.P.; Morse, A.S. Stability of switched systems with average dwell-time. In Proceedings of the 38th IEEE Conference Decision Control (CDC), Phoenix, AZ, USA, 7–10 December 1999; pp. 2655–2660.
20. Zhang, L.; Gao, H. Asynchronously switched control of switched linear systems with average dwell time. *Automatica* **2010**, *46*, 953–958. [CrossRef]
21. Zhai, G.; Hu, B.; Yasuda, K.; Michel, A.N. Stability analysis of switched systems with average dwell time. In Proceedings of the 2000 American Control Conference, Chicago, IL, USA, 28–30 June 2000; pp. 200–204.
22. Liu, J.; Gu, Z.; Park, J.H.; Shen, H. Resilient event-triggered control for networked switched systems under DoS attacks: An average dwell-time approach. *Int. J. Robust Nonlinear Control* **2021**, *31*, 104–122.
23. Wang, J.; Xia, J.; Shen, H.; Wang, Z. H_∞ synchronization for complex dynamical networks with cyber-attacks via event-triggered control. *Appl. Math. Comput.* **2021**, *406*, 126291.
24. Hu, S.; Yue, D.; Xie, X.; Chen, X. Resilient event-triggered control for networked control systems under periodic DoS attacks. *Inf. Sci.* **2019**, *481*, 124–135.
25. Sun, J.; Wang, C.; Sun, C. Resilient quantized control of networked control systems under DoS attacks. *IEEE Trans. Syst. Man Cybern. Syst.* **2021**, *51*, 5345–5354.
26. Ding, D.; Han, Q.-L.; Ge, X.; Wang, J. Secure State Estimation and Control of Cyber-Physical Systems: A Survey. *IEEE Trans. Syst. Man Cybern. Syst.* **2021**, *51*, 176–190. [CrossRef]
27. Hu, T.; Shi, M.; Shi, K.; Wuliu, X. Hybrid impulsive and event-triggered intermittent guaranteed cost secure consensus control for multiagent systems under DoS attacks. *Commun. Nonlinear Sci. Numer. Simul.* **2026**, *158*, 109857. [CrossRef]
28. Wang, X.; Yin, Z.; Lei, Y.; Huang, T.; Kurths, J. Secure Consensus for Switched Multiagent Systems Under DoS Attacks: Hybrid Event-Triggered and Impulsive Control Approach. In *IEEE Transactions on Cybernetics*; IEEE: New York, NY, USA, 2025. [CrossRef] [PubMed]
29. Gao, Y.; Li, X.; Cao, J. Input-to-state stability of switched systems under the new mode-dependent dynamic event-triggered impulsive control. *Int. J. Robust Nonlinear Control* **2025**, *35*, 3715–3727. [CrossRef]
30. Stamova, I.; Stamov, T. *Applied Impulsive Mathematical Models*; Springer: Cham, Switzerland, 2016.
31. Khalil, H.K. *Nonlinear Systems*, 3rd ed.; Prentice Hall: Upper Saddle River, NJ, USA, 2002.
32. Boyd, S.; El Ghaoui, L.; Feron, E.; Balakrishnan, V. *Linear Matrix Inequalities in System and Control Theory*; SIAM: Philadelphia, PA, USA, 1994.

33. Hardy, G.H.; Littlewood, J.E.; Pólya, G. *Inequalities*, 2nd ed.; Cambridge University Press: Cambridge, UK, 1952.
34. Löfberg, J. YALMIP: A toolbox for modeling and optimization in MATLAB. In Proceedings of the 2004 IEEE International Conference on Robotics and Automation, Taipei, Taiwan, 26 April–1 May 2004; pp. 284–289.
35. MOSEK ApS. *The MOSEK Optimization Toolbox for MATLAB Manual, Version 10.0*; MOSEK ApS: Copenhagen, Denmark, 2023. Available online: https://www.mosek.com (accessed on 7 April 2026).

Disclaimer/Publisher's Note: The statements, opinions and data contained in all publications are solely those of the individual author(s) and contributor(s) and not of MDPI and/or the editor(s). MDPI and/or the editor(s) disclaim responsibility for any injury to people or property resulting from any ideas, methods, instructions or products referred to in the content.